applied optics

Experimental evaluation of a 3D wavelet-based phase recovery method in temporal speckle pattern interferometry

Gustavo E. Galizzi,[1,*] Alejandro Federico,[2] and Guillermo H. Kaufmann[1]

[1]Instituto de Física Rosario, Blvd. 27 de Febrero 210 bis, S2000EZP, Rosario, Argentina
[2]Electrónica e Informática, Instituto Nacional de Tecnología Industrial, P.O. Box B1650WAB, B1650KNA, San Martín, Argentina
*Corresponding author: galizzi@ifir-conicet.gov.ar

Received 27 December 2016; revised 30 April 2017; accepted 30 April 2017; posted 1 May 2017 (Doc. ID 283442); published 17 May 2017

We test the performance of a phase recovery method based on a three-dimensional directional wavelet transform applied to the intensity signal measured by temporal speckle pattern interferometry (TSPI). We present and discuss several sources of uncertainty by analyzing experimental datasets recorded for an in-plane interferometer without introducing a temporal carrier. The dynamic phase data measured with the proposed method are compared with those obtained from the well-known one-dimensional Fourier transform phase recovery technique. In the Fourier method, the filtered Fourier transform for each intensity pixel is evaluated along the temporal direction. In contrast, the three-dimensional directional wavelet transform method uses the information of adjacent pixels and then increases the performance of the recovered dynamic phase results. The advantages and limitations of the three-dimensional directional wavelet transform approach are discussed, and a summary of conclusions from the analysis of TSPI data is also given.

OCIS codes: (120.6160) Speckle interferometry; (120.5050) Phase measurement; (100.7410) Wavelets.

https://doi.org/10.1364/AO.56.004412

1. INTRODUCTION

Temporal speckle pattern interferometry (TSPI) is a well-known non-destructive and whole-field optical technique for the measurement of small dynamic deformation fields of rough objects. In this technique, a sequence of speckle interferograms is recorded throughout the entire dynamic deformation process of the tested object. The dynamic field corresponding to the optical phase is related to the undergone object deformation and coded in the spatiotemporal intensity modulation of the recorded speckle pattern interferograms. The collected interferograms are commonly analyzed for each observed pixel independently of the rest. Consequently, most phase recovery approaches developed for TSPI data processing deal with one-dimensional (1D) signals, and their implementation is simple and computationally efficient [1]. However, 1D methods usually present low tolerance to the presence of noise, including errors produced by decorrelation effects, fluctuations of the bias, and loss of modulation intensity. These disadvantages are a severe limitation of the 1D methods, which is a direct consequence of the nature of the dynamic of the intensity signal. The interferometric signal is composed by the dynamic interference of speckle patterns. Therefore, non-modulated or very low modulated pixels, as well as biased intensity fluctuations, are usually obtained. In order to overcome these limitations, various 1D phase recovery techniques based on the Fourier transform, the continuous wavelet transform, the empirical mode decomposition, the Hilbert transform, and the generalized S-transform have been developed [2]. These methods can only consider the state of the interferometric signal before and after the time analyzed. Therefore, there is some potential for development of a more robust temporal method. Note that no information about the neighboring pixels of the analyzed pixel is considered in the mentioned methods and therefore this information is discarded. Alternatively, a technique that combines the use of a 1D method with 2D spatial phase evaluation was proposed [3]. This technique allows the analysis of discontinuous phase maps together with varying changes of phase.

In practice, 1D methods fail in the presence of a significant number of neighboring unmodulated pixels. Consequently, 2D and 3D approaches that consider information of adjacent pixels have been investigated, such as a technique based on Delaunay triangulation [4]. This approach removes signal intervals according to a user-defined criterion and then, the missing data are rebuilt by interpolation. Finally, the phase is evaluated using the Hilbert transform. Alternatively, the 3D directional wavelet transform method (3DDWT) was proposed as a phase recovery technique in order to deal with the loss of modulation with

minimum intervention of an external operator [2,5]. In addition, this technique allows the evaluation of displacement fields with different directions, the analysis of discontinuous phase maps, and variations of changes of phase by adopting a single set of external parameters fixed by the operator.

In this work, we experimentally evaluate the performance of the 3DDWT phase evaluation method using experimental TSPI datasets recorded from a nanopositioner-controlled object that produces a rigid body in-plane movement with high excursions. Additionally, we compare the performance obtained with the one given by the well-known 1D Fourier transform method [6]. The results obtained by these techniques are compared for different phase distributions, and the advantages and limitations of both temporal phase recovery approaches are also discussed. It is necessary to point out that no temporal carrier was introduced in the optical setup for the recording of the speckle interferograms. In this way, the uncertainties associated with this approach are avoided because it is unnecessary to subtract the carrier component in the final phase recovery calculation. Note that the interferometric signal is contaminated with low-frequency noise and intensity biases, and then the selection of the set of parameters is more laborious.

2. PHASE RECOVERY METHODS IN TSPI

When a series of speckle interferograms is acquired in a TSPI experiment without introducing a temporal carrier in the interferometer, the intensity distribution I at pixel coordinates (m, n) and time t can be written as [1]

$$I(m, n, t) = I_B(m, n, t) + I_M(m, n, t)\cos[\varphi(m, n, t)], \quad (1)$$

where I_B and I_M are the bias and modulation intensities, respectively, and φ is the phase to be recovered. It should be noticed that $\varphi(m, n, t = 0)$ is an initial random phase value that has to be subtracted from φ in order to obtain the final dynamic phase change distribution.

In the following subsections, the phase recovery algorithms corresponding to both 1D Fourier transform and 3D directional wavelet transform methods are briefly described for convenience of the readers.

A. One-Dimensional Fourier Transform Method

Evaluating the Fourier transform of the intensity I along the time axis in Eq. (1), $\tilde{I}(\omega)$ results in [2]

$$\begin{aligned}\tilde{I}(\omega) &= \mathrm{FT}\{I(t)\}(\omega)\\ &= \mathrm{FT}\{I_B(t)\}(\omega) + \mathrm{FT}\left\{\frac{I_M(t)}{2}\exp[j\varphi(t)]\right\}(\omega)\\ &\quad + \mathrm{FT}\left\{\frac{I_M(t)}{2}\exp[-j\varphi(t)]\right\}(\omega), \end{aligned} \quad (2)$$

where j is the imaginary unit, FT stands for the Fourier transform operator, and ω is the frequency in Fourier space. As each pixel of the image sequence is analyzed independently of all the others, the dependence of the magnitudes in the spatial coordinates m and n was omitted for the sake of clarity.

The last two terms in Eq. (2) include the phase to be recovered, which can be isolated by applying an appropriate bandpass filter [1]. Then, the resulting complex intensity signal $U(t)$ is evaluated applying the inverse Fourier transform as follows:

$$U(t) = \mathrm{FT}^{-1}\{H(\omega, F_L, F_H)\tilde{I}(\omega)\}(t), \quad (3)$$

where FT^{-1} stands for the inverse Fourier transform operator and H is the transfer function in the frequency domain of the applied bandpass filter with low and high cutoff frequencies F_L and F_H, respectively. Finally, the dynamic phase φ of the object at the deformed state can be calculated at each pixel using the arctangent function atan2(·,·) as follows:

$$\begin{aligned}\varphi(t) &= \mathrm{atan\,2}(\mathrm{Im}\{U(t)\}, \mathrm{Re}\{U(t)\})\\ &\quad - \mathrm{atan\,2}(\mathrm{Im}\{U(0)\}, \mathrm{Re}\{U(0)\}), \end{aligned} \quad (4)$$

where atan2(·,·) is the four-quadrant inverse tangent function which return values in the closed interval $(-\pi, \pi)$ based on the values of its arguments, and Im{·} and Re{·} denote the imaginary and real part of the complex U, respectively.

B. Three-Dimensional Directional Wavelet Transform Method

The 3D directional wavelet transform D_I of the TSPI intensity distribution $I(m, n, t) = I(\mathbf{x})$ [see Eq. (1)] can be evaluated as [2,5]

$$D_I(a, \mathbf{b}) = C_\psi \frac{1}{a}\int_{-\infty}^{+\infty} I(\mathbf{x})\psi * \left[\frac{1}{a}(\mathbf{x} - \mathbf{b})\right]\mathrm{d}\mathbf{x}, \quad (5)$$

where $\mathbf{x} = (m, n, t) \in \mathbb{R}^3$ is the spatial-temporal coordinate and $\mathbb{R}$ denotes the set of real numbers, $\psi(\mathbf{x})$ is the three-dimensional analyzing wavelet, * stands for the complex conjugate operator, $a > 0$ is the dilation or scaling parameter, $\mathbf{b} = (m_b, n_b, t_b) \in \mathbb{R}^3$ is the displacement or translation parameter, and C_ψ is a normalizing constant. As the wavelet ψ is translated by $\mathbf{b}$ and dilated by a, D_I can be considered as the convolution of $I(\mathbf{x})$ and $\psi(\mathbf{x})$ in the variables $(a, \mathbf{b})$. In this way, D_I acts as local filter on the intensity signal $I(\mathbf{x})$ and has an appreciable value where local features of the intensity I are matched. It should be noted that Eq. (5) is a convolution product with a zero-mean function ψ and therefore its fully spaced representation can be discretized as usual by using Fourier-transform-based procedures.

To measure the time evolution of the phase coded in the TSPI signal, a wavelet that separates the amplitude and phase components can be used. In particular, we use the modified Morlet wavelet defined as [2,5]

$$\begin{aligned}\psi(m, n, t) &= \psi_G \times \psi_M\\ &= \exp\left\{-\left[\left(\frac{m}{\sigma_m}\right)^2 + \left(\frac{n}{\sigma_n}\right)^2\right]/2\right\}\\ &\quad \times \exp\left[-\left(\frac{t}{\sigma_t}\right)^2/2\right]\exp(jk_0 t), \end{aligned} \quad (6)$$

where ψ_G is a 2D spatial Gaussian function; ψ_M is the 1D temporal Morlet wavelet; and σ_m, σ_n, σ_t, and k_0 are adjusting parameters. The value of k_0 is associated with the Morlet frequency and σ_m, σ_n, σ_t correspond to the effective window width of the wavelet function in each magnitude. In the fully spaced representation, Eq. (6) is a convex cone centered at frequency k_0. Variations of the external parameters modify the angular selectivity and then the spectral anisotropy can be better adapted obtaining high performance in the phase recovery process. In Section 3 we offer typical values of these parameters

as a reference for the interested reader. From Eqs. (5) and (6), D_I can be seen as a convolution of I with a 2D spatial Gaussian filter and the 1D wavelet transform of the temporal history of each pixel in the image sequence [2,5].

The tracking of the local maximum of $|D_I(a, \mathbf{b})|$ allows the characterization of the ridge a_r, which has the property of describing the phase distribution evolution as follows:

$$\varphi(\mathbf{b}) = \operatorname{atan2}(\operatorname{Im}\{D_I(a_r, \mathbf{b})\}, \operatorname{Re}\{D_I(a_r, \mathbf{b})\}) - \operatorname{atan2}(\operatorname{Im}\{D_I(a_r, \mathbf{b}_0)\}, \operatorname{Re}\{D_I(a_r, \mathbf{b}_0)\}), \quad (7)$$

where $\mathbf{b}_0 = (m, n, 0)$. Finally, a 1D phase unwrapping algorithm along the temporal direction is needed to recover the continuous phase distribution.

3. EXPERIMENTAL RESULTS

We evaluated the experimental performance of the 3DDWT phase recovery technique and carried out a comparison of the obtained results with those calculated applying the 1D Fourier transform method. For this purpose, we set different experimental conditions and acquired the corresponding datasets by using a speckle interferometer with in-plane sensitivity. As previously mentioned, no temporal carrier was added to the optical setup during the recording of the speckle interferograms, so as to avoid the uncertainties introduced by the characteristic method used in carrier subtraction to obtain the final dynamic phase results. One important drawback of this experimental approach is that the interferometric signals are contaminated with noise composed of low frequencies and intensity biases, making it difficult to select the appropriate bandpass filter needed for the 1D Fourier method and the ridge tracking procedure parameters for the 3DDWT technique. The measured displacement fields were monotonically increasing with time and conserving its spatial geometry to exclude the ambiguity problem in the phase sign. Also, a structural similarity index was defined for the evaluation of the recovered phase variations.

Figure 1 shows a diagram of the experimental setup of the TSPI system used in the experiments. The light from a He–Ne laser with a wavelength $\lambda = 632.8$ nm is divided into two beams by a 50/50 beam splitter. Both beams are expanded by two microscope objectives and illuminate the specimen (S) making an angle $\theta = 45°$ with respect to the normal of the surface. It is necessary to point out that both microscope objectives were placed far enough from S so that the sensitivity vector can be considered constant over the 8 mm × 8 mm area analyzed. The specimen is a 3 cm × 4 cm aluminum plate attached to a Physik Instrumente P-611.Z Z Stage (NP). A Physik Instrumente E-625 Servo-Controller acted as the control unit (CU) which applies a voltage to the nanopositioner using an open loop control scheme. The applied voltage generates a displacement of the specimen that is the same for every point of the object surface. The specimen is imaged by a PULNIX TM-620 CCD camera whose output is fed to a frame grabber located inside a personal computer. Both the image acquisition system and the CU, which generates the displacement of the NP, are controlled by the personal computer. The resolution of the acquired images was 128 × 128 pixels and 256 gray levels, and each dataset contained 512 images. The mean

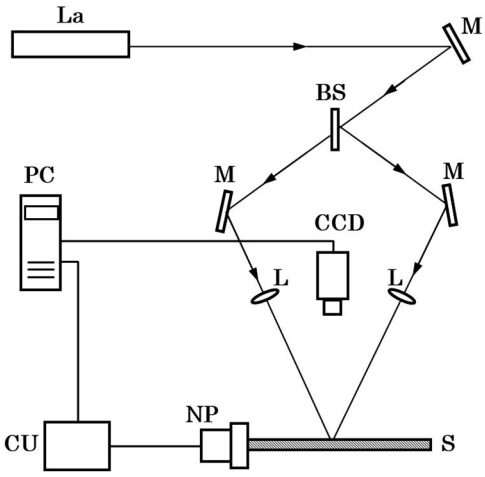

Fig. 1. TSPI system used to obtain the in-plane displacement datasets: La, He-Ne laser; BS, beam splitter; M, mirrors; L, microscope objectives; CCD, video camera; S, specimen; NP, nanopositioner; CU, control unit; PC, personal computer.

speckle size in the acquired images was approximately 1.3 pixels, and no intensity saturation was detected during the whole data acquisition. The 1D Fourier transform method was implemented using the widely known fast Fourier transform algorithm [1], and the 3DDWT was evaluated using the algorithms available in [7].

Two different phase distributions were studied. First, the CU was programmed to apply a linearly increasing voltage to the NP. This procedure generates a constant temporal variation in the phase to be measured, which corresponds to a rigid body motion. Then, the phase was evaluated using the 1D Fourier transform method with cutoff frequencies $F_L = 24$ and $F_H = 104$, and the 3DDWT technique with adjusting parameters $\sigma_m = \sigma_n = 1$, $\sigma_t = 3$, and $k_0 = 4$.

Figure 2 depicts the temporal history of the intensity signal registered for the central pixel of the image corresponding to a programmed phase change $\Delta\varphi_P$ of nearly $\pi/4$ rad between successive frames.

Figure 3 shows the temporal evolution of the programmed phase φ_P (dotted line), and the phases evaluated for the central

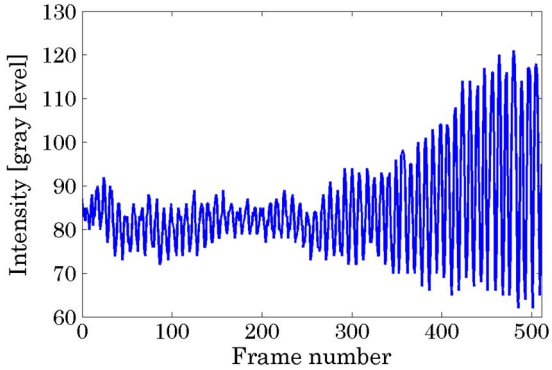

Fig. 2. Temporal history of the intensity recorded for a pixel of the image sequence corresponding to a programmed phase change of approximately $\pi/4$ rad per frame.

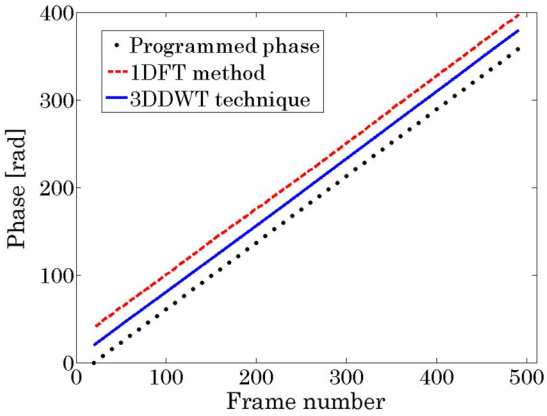

Fig. 3. Temporal evolution of the programmed phase (dotted line), and the phase distributions evaluated for the central pixel of the image using the 1D Fourier transform method (dashed line) and the 3DDWT technique (solid line), corresponding to a programmed phase change of approximately $\pi/4$ rad per frame. A constant phase was added to both recovered phase distributions for the sake of clarity.

pixel of the image (see Fig. 2) using the 3DDWT technique (solid line) and the 1D Fourier transform method (dashed line). A constant phase was added to both recovered phase distributions for the sake of clarity. It can be seen that there is a close agreement in the evaluated phase values using both methods.

Figure 4 depicts the phase recovered with the 3DDWT technique for pixels along the central column of the image. It can be seen that the change of phase is approximately constant along the time axis and similar for every pixel located in the column.

In order to compare the overall performance of both phase evaluation techniques, we defined the average similarity S_A as follows:

$$S_A = \frac{1}{N_f}\sum_{t_n=0}^{N_f-1} S_{MR}(t_n), \tag{8}$$

where N_f is the total number of acquired frames, t_n is the frame number, and $S_{MR}(t_n)$ is the structural similarity index (SSIM) [8] evaluated at frame t_n. S_{MR} measures the similarity between the images M and R. In particular, the SSIM index can be viewed as a statistic quality measure of M being compared to

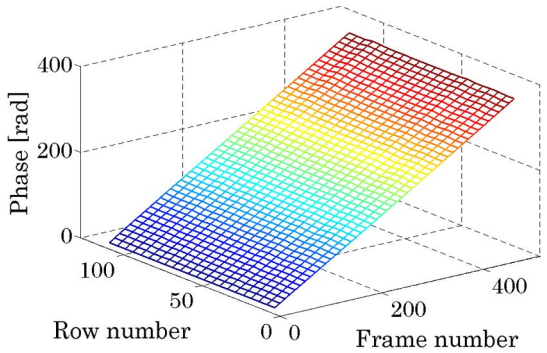

Fig. 4. Temporal evolution of the phase distribution evaluated using the 3DDWT technique for pixels along the central column of the images, corresponding to a phase change of nearly $\pi/4$ rad per frame.

R, which is regarded as being of perfect quality. In our case, M is the recovered phase value at each frame and R is the estimated phase value, which was calculated by linearly fitting the mean value of the recovered phase in complete agreement with the NP voltage programmed for the rigid body motion.

The SSIM index is first evaluated locally within a sliding window that moves on a pixel basis across the entire image area, generating a SSIM map. The local SSIM index $LS(w_M, w_R)$ accounts for the similarity in luminance l, contrast c, and structure s within the sliding windows w_M and w_R taken from the same location of both M and R, and is computed as [8]

$$\begin{aligned} LS(w_M, w_R) &= l(w_M, w_R) \times c(w_M, w_R) \times s(w_M, w_R) \\ &= \left(\frac{2\mu_M\mu_R + C_1}{\mu_M^2 + \mu_R^2 + C_1}\right) \times \left(\frac{2\sigma_M\sigma_R + C_2}{\sigma_M^2 + \sigma_R^2 + C_2}\right) \\ &\quad \times \left(\frac{\sigma_{MR} + C_3}{\sigma_M\sigma_R + C_3}\right), \end{aligned} \tag{9}$$

where μ_M and μ_R are the local mean values of w_M and w_R, σ_M and σ_R are the variances of w_M and w_R, σ_{MR} is the cross correlation of w_M and w_R after removing their means, and C_1, C_2, and C_3 are small positive constants to stabilize each term. Finally, S_{MR} is the average of the generated LS values [9]. It is necessary to point out that $-1 \le LS \le 1$, being $LS = 1$ if w_M and w_R are identical. In addition, $LS(w_M, w_R) = LS(w_R, w_M)$ so that the index value is the same regardless the order of the image comparison. The same remarks are valid for S_{MR} and S_A. For the interested reader, the SSIM index was evaluated using the algorithms available in [10]. It is necessary to point out that the outer 10 pixels of every image and the 20 first and last frames were excluded for the computation of S_{MR} and S_A.

The experiment was repeated in the same way but using different $\Delta\varphi_P$ values from approximately $\pi/11$ up to $\pi/2$ rad, and the obtained S_A results are summarized in Table 1. It can be noticed that the performances of both techniques are quite similar.

It is important to remark that the adjusting parameters of the 3DDWT technique were fixed once for the complete evaluation of all experimental datasets. The cutoff frequency parameters of the bandpass filter corresponding to the 1D Fourier transform method had to be determined for each dataset with the intervention of an experienced operator. Particularly, the cutoff frequency parameters of the bandpass filter were chosen so as to obtain an acceptable performance of the 1D Fourier transform method.

Afterward, a region of 128 × 128 pixels containing two low modulation intensity areas was analyzed using the recorded dataset corresponding to $\Delta\varphi_P \approx \pi/4$ rad between successive frames. The size of each low modulation area was nearly

Table 1. S_A Values Obtained for Different $\Delta\varphi_P$

	S_A	
$\Delta\varphi_P$	1D Fourier Transform	3DDWT
$\pi/2$	0.99	0.99
$\pi/3$	0.98	0.98
$\pi/4$	0.98	0.99
$\pi/11$	0.97	0.96

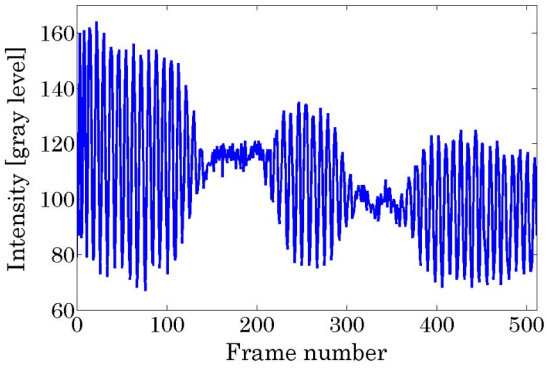

Fig. 5. Temporal evolution of the intensity corresponding to a pixel with low-intensity modulation.

43 × 43 pixels. Figure 5 depicts the temporal history of the intensity of a pixel with poor intensity modulation belonging to the analyzed area. It can be noticed that the loss of intensity modulation occurred around the frames 150 and 320 approximately. Moreover, note also the high intensity variability corresponding to this particular temporal history of the pixel.

Figure 6 shows the temporal evolution of the phase evaluated for the pixel with poor intensity modulation (see Fig. 5) using the 3DDWT technique (solid line) and the 1D Fourier transform method (dashed line). It can be seen that some errors occurred in the phase recovered with the Fourier transform method when the intensity modulation is close to its minimum. On the other hand, the 3DDWT technique was not noticeably affected by the poor modulation: the recovered phase values are similar to the ones shown in Fig. 3.

Figure 7 depicts the temporal evolution of the structural similarity index S_{MR} evaluated for the recovered phase using the 3DDWT technique (solid line) and the 1D Fourier transform method (dashed line) corresponding to the dataset containing low modulation intensity areas.

Even though the values of S_{MR} obtained with both techniques were close to 1, the performance of the 1D Fourier transform method is more affected by low modulation intensity

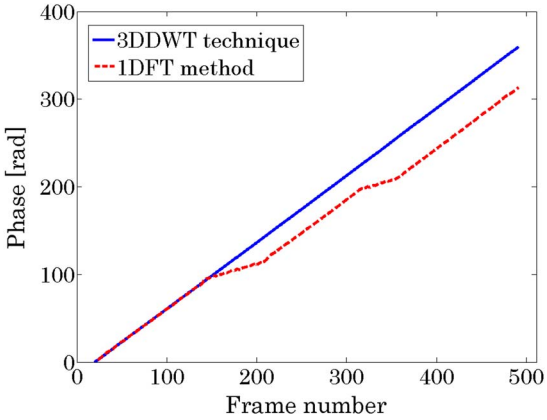

Fig. 6. Temporal evolution of the phase distribution evaluated using the 3DDWT technique (solid line) and the 1D Fourier transform method (dashed line) corresponding to a pixel with poor intensity modulation.

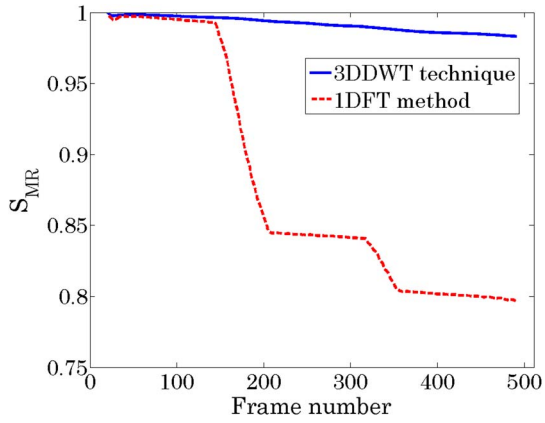

Fig. 7. Temporal evolution of the structural similarity index SMR evaluated for the recovered phase using the 3DDWT technique (solid line) and the 1D Fourier transform method (dashed line) corresponding to the dataset containing low modulation intensity areas.

regions than the 3DDWT technique. We remark that the bandpass filter and the adjusting parameter values were fixed at the original and poor modulation datasets.

In a similar way, the performance of both techniques was evaluated using different $\Delta\varphi_P$ values and the obtained S_A results are summarized in Table 2. It can be noticed that the 3DDWT technique outperforms the 1D Fourier transform method and is not noticeably affected by the low modulation of the intensity (see Table 1).

Finally, the performance of both phase retrieval techniques was tested when the variation of the phase change $\Delta\varphi_P$ decreases with time. In this case, the programmed phase function φ_P at frame t_n was

$$\varphi_P(t_n) = \left\{\exp\left[\left(\frac{1}{2}\right)^5\right] - \exp\left[\left(\frac{1}{2} - \frac{t_n}{2N_f}\right)^5\right]\right\} M_\varphi, \quad (10)$$

where $M_\varphi = 3665$ rad is an adjusting parameter. The value of M_φ was chosen to make the maximum temporal variation of the phase less than π, so that the temporal phase was properly sampled by the acquisition system. In this case, the phase was evaluated using the 1D Fourier transform method with the cutoff frequencies $FL = 1$ and $F_H = 160$, and the 3DDWT with the adjusting parameters $\sigma_m = \sigma_n = 1$, $\sigma_t = 6$, and $k_0 = 0.1$.

Figure 8 shows the temporal history of the intensity signal registered for a pixel of the image sequence corresponding to a monotonic non-constant phase change.

Figure 9 depicts the temporal evolution of the programmed phase φ_P (dotted line), and the temporal histories of the phase

Table 2. S_A Values Obtained for Low Modulated Intensity Signals

	S_A	
$\Delta\varphi_P$	1D Fourier Transform	3DDWT
$\pi/2$	0.94	0.98
$\pi/3$	0.84	0.98
$\pi/4$	0.88	0.99
$\pi/11$	0.86	0.95

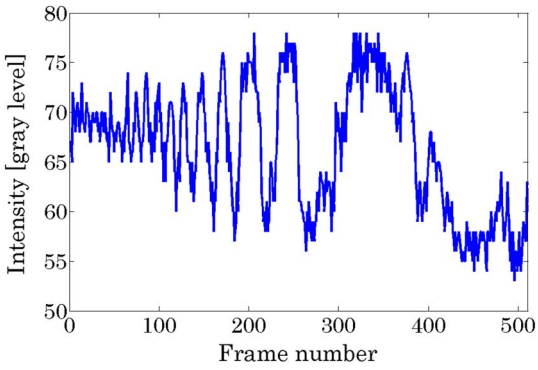

Fig. 8. Temporal history of the intensity recorded for a pixel of the image sequence corresponding to a monotonic non-constant phase change.

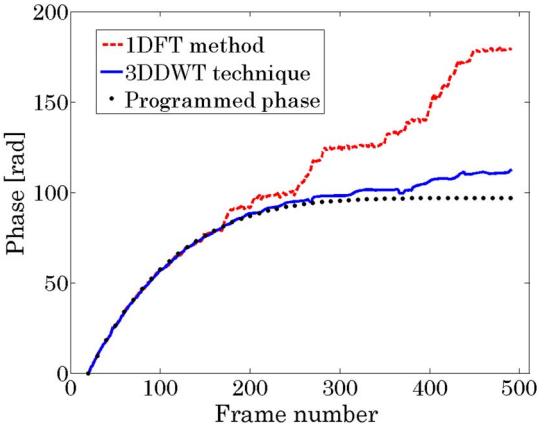

Fig. 9. Temporal evolution of the programmed phase (dotted line), and the phase distributions evaluated for the central pixel of the image sequence using the 3DDWT technique (solid line) and the 1D Fourier transform method (dashed line) corresponding to a monotonic non-constant phase change.

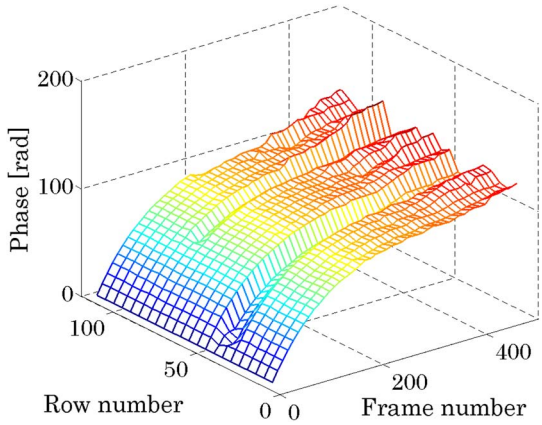

Fig. 10. Temporal evolution of the phase distribution evaluated using the 3DDWT technique for pixels along the central column of the images, corresponding to a monotonic non-constant phase change.

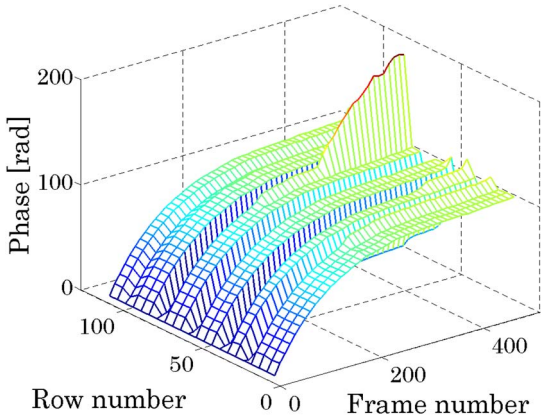

Fig. 11. Temporal evolution of the phase distribution evaluated using the 1D Fourier transform method for pixels along the central column of the images, corresponding to a monotonic non-constant phase change.

distributions recovered for the central pixel of the image (see Fig. 8) using the 3DDWT technique (solid line) and the 1D Fourier transform method (dashed line) corresponding to a monotonic non-constant phase change [see Eq. (10)]. It is noted that both phase retrieval techniques allow the evaluation of the phase distribution with lower errors when the phase changes per frame are sufficiently large. However, when the phase change becomes very small, such as after frame 250, both phase evaluation techniques have problems to recover the phase distribution, although the errors introduced by the 3DDWT technique are much smaller than those given by the 1D Fourier transform method.

Figure 10 shows the phase distribution obtained with the 3DDWT technique for pixels along the central column of the image. It can be seen that the temporal history of the recovered phase is similar for most of the pixels located along the column and that the phase errors are more noticeable after frame 250.

Figure 11 depicts the recovered phase with the 1D Fourier transform method for pixels along the central column of the image. It is noted that the temporal history of the recovered phase is similar for many pixels in the column, but the phase errors are larger than those obtained using the 3DDWT technique (see Figs. 9 and 10). The 1D Fourier transform method is more prone to produce errors in the recovered phase when it is compared with the 3DDWT technique.

4. CONCLUSIONS

We evaluated the performance of the 3DDWT technique in practice and compared the obtained results with those given by the well-known 1D Fourier transform method when both approaches are used to retrieve phase distributions in TSPI. For this purpose, different dynamic phase distributions were used with their corresponding experimental TSPI datasets. In the case of low-intensity modulation and when the phase change is very small, the 3DDWT technique improves the estimation of the recovered dynamic phase distributions with respect to the 1D Fourier transform method. The performance of both the 1D Fourier transform method and the 3DDWT technique

depends on the selection of their parameters. The parameters of the 3DDWT technique were fixed for all the experimental datasets whereas the cutoff frequencies of the bandpass filter corresponding to the 1D Fourier transform method were determined for each particular case to obtain an acceptable performance. Therefore, the application of the 3DDWT technique is less operator-dependent and robust to analyze different TSPI datasets. Another topic for a future investigation related to this study is the automatic setting of the configuration parameters of the 3DDWT technique, particularly in the case of strong alterations in the change of phase variations.

Funding. Consejo Nacional de Investigaciones Científicas y Técnicas (CONICET) (PIP11220110100971).

Acknowledgment. We wish to thank the reviewers for many useful comments that have helped to improve this publication.

REFERENCES

1. J. M. Huntley, "Automated analysis of speckle interferograms," in *Digital Speckle Pattern Interferometry and Related Techniques*, P. K. Rastogi, ed. (Wiley, 2001), pp. 59–139.
2. A. Federico and G. H. Kaufmann, "Phase evaluation in temporal speckle pattern interferometry using time-frequency methods," in *Advances in Speckle Metrology and Related Techniques*, G. H. Kaufmann, ed. (Wiley, 2011), pp. 147–205.
3. J. Burke and H. Helmers, "Matched data storage in ESPI by combination of spatial phase shifting with temporal phase unwrapping," Opt. Laser Technol. **32**, 235–240 (2000).
4. S. Equis and P. Jacquot, "Coping with low modulation in speckle interferometry: a novel approach based on Delaunay triangulation," Proc. SPIE **7387**, 738709 (2010).
5. A. Federico and G. H. Kaufmann, "Robust phase recovery in temporal speckle pattern interferometry using a 3D directional wavelet transform," Opt. Lett. **34**, 2336–2338 (2009).
6. M. Takeda, H. Ina, and S. Kobayashi, "Fourier transform method of fringe analysis for computer based topography and interferometry," J. Opt. Soc. Am. **72**, 156–160 (1982).
7. L. Jacques, A. Coron, P. Vandergheynst, and A. Rivoldini, "The YAWTb Toolbox: Yet Another Wavelet Toolbox [software] (2007)," http://sites.uclouvain.be/ispgroup/yawtb/.
8. Z. Wang, A. C. Bovik, H. M. Sheikh, and E. P. Simoncelli, "Image quality assessment: from error visibility to structural similarity," IEEE Trans. Image Process. **13**, 600–612 (2004).
9. Z. Wang and A. C. Bovik, "Mean squared error: love it or leave it?" IEEE Signal Process. Mag. **26**, 98–117 (2009).
10. Z. Wang, A. C. Bovik, H. M. Sheikh, and E. P. Simoncelli, "The SSIM Index for Image Quality Assessment [software] (2011)," http://www.cns.nyu.edu/~lcv/ssim/.